NANO LETTERS

Letter

pubs.acs.org/NanoLett

Anisotropic, Hierarchical Surface Patterns via Surface Wrinkling of Nanopatterned Polymer Films

Jung-Hyun Lee,[†,∥] Hyun Wook Ro,[*,†] Rui Huang,[‡] Paul Lemaillet,[§,⊥] Thomas A. Germer,[§] Christopher L. Soles,[†] and Christopher M. Stafford[*,†]

[†]Polymers Division, National Institute of Standards and Technology, 100 Bureau Drive, Gaithersburg, Maryland 20899, United States

[‡]Department of Aerospace Engineering and Engineering Mechanics, University of Texas, Austin, Texas 78712, United States

[§]Sensor Science Division, National Institute of Standards and Technology, 100 Bureau Drive, Gaithersburg, Maryland 20899, United States

[⊥]Institute for Research in Electronics and Applied Physics, University of Maryland, College Park, Maryland 20742, United States

S *Supporting Information*

ABSTRACT: By combining surface wrinkling and nanopatterned polymer films, we create anisotropic, hierarchical surfaces whose larger length-scale (wrinkling wavelength) depends intimately on the geometry and orientation of the smaller length-scale (nanopattern). We systematically vary the pattern pitch, pattern height, and residual layer thickness to ascertain the dependence of the wrinkling wavelength on the nanopattern geometry. We apply a composite mechanics model to gain a quantitative understanding of the relationship between the geometric parameters and the anisotropy in wrinkling wavelength. Additionally, these results shed light on the effect of surface roughness, as represented by the nanopattern, on the metrology of thin films via surface wrinkling.

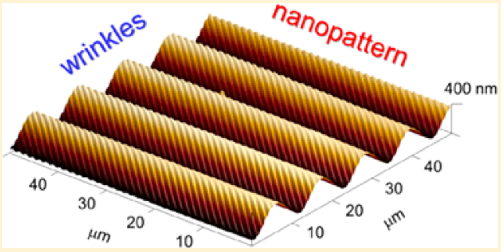

KEYWORDS: *Polymeric materials, thin films, patterning, nanostructures, hierarchical structures, metrology*

Scientists have long been inspired by hierarchical surfaces found in nature—the classic example being the Lotus leaf. The Lotus leaf exhibits a papillae microstructure coated with a nanostructured tubular wax, which in combination grants the surface of the Lotus leaf superhydrophic and self-cleaning properties.[1] Drawing from this inspiration, researchers have designed artificial hierarchical surfaces by a variety of methods, including lithography,[2−4] replica molding,[5] etching,[6] chemical deposition,[7,8] and colloidal assembly.[9,10] Recently, there has been growing interest in creating hierarchical surfaces using surface wrinkling of a stiff skin on an elastomeric substrate due to its spontaneous nature, tunability, versatility, and ability to generate large area patterns. For example, Efimenko et al.[11] demonstrated that compressing oxidized polydimethylsiloxane (PDMS) at high strains leads to the formation of nested, hierarchical wrinkled surfaces having generations of wrinkles that spanned 3 orders of magnitude in length scales from tens of nanometers to hundreds of micrometers. Similarly, Chiche et al.[12] employed sequential oxidation, wrinkling, and replication of PDMS to create a checkerboard-like pattern consisting of orthogonal wrinkling patterns having slightly different length-scales in two directions, while Davis and Crosby used a two-step curing process of PDMS and sequential strain fields to create a range of biaxial wrinkle morphologies.[13] To date, most studies involving wrinkling to create multilength scale patterned surfaces rely on plasma oxidation or ultraviolet-ozonolysis (UVO) to create a stiff skin. While these approaches are quite practical, the thickness and mechanical properties of the resulting skin layer are largely unknown due to its depth-heterogeneous structure, making quantitative understanding of the resulting patterns nearly impossible. Furthermore, there has been limited success in making well-controlled anisotropic hierarchical morphologies where the orientation of one pattern with respect to the other can be easily tuned.

We report here a facile method for creating hierarchical patterns by surface wrinkling of a prepatterned polymer film. By employing a prepatterned polymer film, we can easily measure the exact thickness and modulus of the patterned surface consisting of a uniform material and thus can model the effect of pattern dimensions and layer thicknesses on the resultant wrinkling periodicity. A schematic of the procedure is depicted in Figure 1. The first length-scale pattern was generated by spin-casting a polymer solution on a silicon template to replicate periodic one-dimensional (1-D) nanopatterns into polystyrene (PS) films and subsequently transferring the patterned PS films onto prestrained PDMS (Figure 1a). A variety of geometric parameters such as residual film thickness (h_1), pattern height (h_2), and pitch size (d) of the nanopatterned PS films were prepared by varying solution concentration and template geometry, while keeping the area fraction of the pattern (defined by the line-to-space ratio, L/S)

Received: September 20, 2012
Published: October 22, 2012

   dx.doi.org/10.1021/nl303512d | *Nano Lett.* 2012, 12, 5995−5999

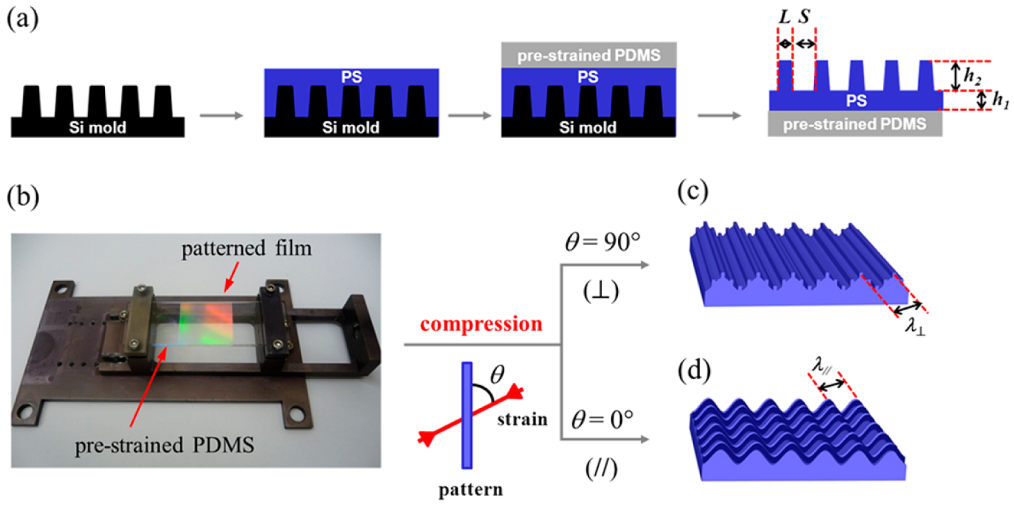

Figure 1. (a) Schematic of the approach for producing nanopatterned PS films via spin-casting directly atop a lithographically patterned mold and subsequently transferring to the surface of PDMS. (b) Optical image of the patterned PS film on the prestrained PDMS. The release of the prestrain leads to wrinkling of the patterned film, where the pattern can be either (c) perpendicular or (d) parallel to the compression direction depending on the relative film orientation.

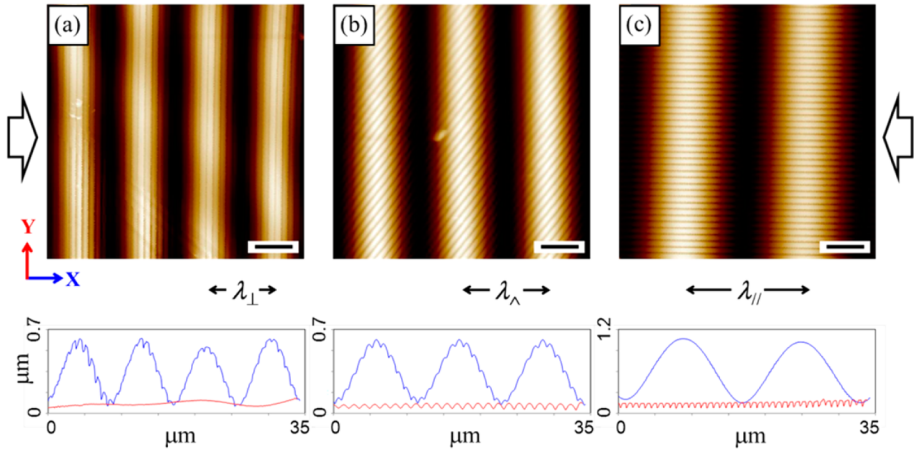

Figure 2. AFM images and corresponding line profiles of wrinkled nanopatterned PS films with varying angles (θ) between the pattern direction and the compression direction: (a) 90° (⊥), (b) 45° (∧), and (c) 0° (//). In the line profiles, the blue traces are taken from a line scan going left to right, while the red traces are top to bottom. The residual layer thickness (h_1) and pattern height (h_2) are identical in all three cases. The scale bars represent 5 μm.

constant. The second length-scale pattern was created by surface wrinkling of the PS/PDMS bilayer. Upon releasing the applied prestrain, a uniform wrinkling pattern with well-defined wavelength (λ) was generated orthogonal to the compression direction while preserving the replicated line-and-space pattern, resulting in a dual length-scale surface consisting of the nanoscale line patterns and the microscale wrinkled undulations. In addition, the spatial orientation of the hierarchical patterns was tuned by altering the angle between the compression direction and the line pattern (Figure 1b–d) to create anisotropic, hierarchical surfaces.

Figure 2 shows atomic force microscopy (AFM) height images and corresponding line profiles of dual length-scale patterns prepared by wrinkling of prepatterned PS films. We prepared three different samples with varying orientation of the nanopatterned PS film with respect to the compression direction, noting that the wrinkling pattern forms orthogonal to the compression direction. In the first case, the compression direction was *perpendicular* to the nanopatterns (θ = 90°), such that the nanopatterns rode atop the wrinkled undulations (Figure 2a). In the second case, the compression direction was *parallel* to the nanopatterns (θ = 0°), such that the nanopatterns spanned across the wrinkled waves (Figure 2c). In the third case, the compression direction was tilted with an angle between the two extremes (θ = 45° in this case, Figure 2b). These images illustrate the ease by which we can produce dual length-scale patterned surfaces with arbitrary orientations between the two patterns. As can be seen from the corresponding line profiles, the wavelength (λ) of wrinkle patterns increased as the compression angle decreased. We observed the smallest wavelength for θ = 90° (⊥) and the largest wavelength for θ = 0° (//). Although a detailed dependence of λ on the compression angle will be reported in a subsequent publication, λ for θ = 45° (∧) corresponded approximately to the average of those induced by perpendicular and parallel compression.

It has been previously shown that the wrinkling behavior of heterogeneously structured films depends on the direction of the applied strain.[14,15] In fact, the compression angle-dependent wrinkling behavior of the surfaces having 1-D nanopatterns

dx.doi.org/10.1021/nl303512d | *Nano Lett.* 2012, 12, 5995–5999

Table 1. Experimentally Measured Wrinkle Wavelengths (λ) Corresponding to the Perpendicular ($\lambda_\perp$) and Parallel Compression ($\lambda_{//}$) Depending on the Geometric Parameters of PS Films with Periodical 1-D Nanopatterns and Their Predicted Values Based on a Composite Model

					experimental		predicted	
d (nm)	h_1 (nm)	h_2 (nm)	λ_{eq} (μm)	λ_1 (μm)	$\lambda_\perp$ (μm)	$\lambda_{//}$ (μm)	$\lambda_\perp$ (μm)	$\lambda_{//}$ (μm)
420	435.2 ± 2.5	51.0 ± 3.1	25.0 ± 0.2	23.4 ± 0.1	25.7 ± 0.8	26.6 ± 0.7	24.8 ± 0.2	25.1 ± 0.2
420	157.1 ± 0.7	45.8 ± 1.0	9.9 ± 0.1	8.4 ± 0.1	9.7 ± 0.3	10.4 ± 0.2	9.5 ± 0.1	10.1 ± 0.1
420	116.9 ± 0.8	45.4 ± 1.0	7.7 ± 0.1	6.3 ± 0.1	6.8 ± 0.2	7.8 ± 0.1	7.2 ± 0.1	8.0 ± 0.1
800	438.9 ± 3.3	49.5 ± 2.1	25.1 ± 0.2	23.6 ± 0.2	26.0 ± 0.9	26.5 ± 0.4	24.9 ± 0.2	25.2 ± 0.3
800	147.0 ± 3.1	50.7 ± 3.9	9.5 ± 0.3	7.9 ± 0.2	9.6 ± 0.3	10.5 ± 0.3	9.0 ± 0.2	9.8 ± 0.3
800	101.7 ± 5.0	55.6 ± 5.9	7.2 ± 0.5	5.5 ± 0.3	6.9 ± 0.3	7.9 ± 0.2	6.4 ± 0.3	7.6 ± 0.5
844	209.7 ± 1.0	186.6 ± 1.9	17.1 ± 0.1	11.3 ± 0.1	13.2 ± 0.3	18.1 ± 0.7	13.5 ± 0.1	19.1 ± 0.1
844	113.8 ± 0.9	203.3 ± 1.5	12.5 ± 0.1	6.1 ± 0.1	7.9 ± 0.6	14.7 ± 0.7	7.3 ± 0.1	15.5 ± 0.1
844	72.1 ± 0.9	204.8 ± 1.8	10.3 ± 0.1	3.9 ± 0.1	4.8 ± 0.3	13.1 ± 0.5	4.3 ± 0.1	13.7 ± 0.1
844	60.7 ± 3.0	198.5 ± 3.4	9.5 ± 0.3	3.3 ± 0.2	4.2 ± 0.4	12.1 ± 0.6	3.7 ± 0.2	13.0 ± 0.3

observed in this work agrees qualitatively with a previous study by Ohzono and Shimomura for the compressive strain-induced pattern rearrangement of preformed stripe wrinkle patterns.[16] It was found that the new wavelength of a rearranged wrinkled pattern increased as the compression angle (θ) with respect to the orientation of the original wrinkled pattern decreased. This behavior was explained by the anisotropy in the effective bending rigidity of films having 1-D wavy surface features, where higher bending rigidities were expected at lower θ.

In addition to the compression angle, the wrinkle wavelength (λ) of such films with periodic surface patterns can be regulated by geometric parameters such as the residual film thickness (h_1), pattern height (h_2), and pitch size (d). For flat films, the wrinkling wavelength is predicted by[17,18]

$$\lambda = 2\pi h_f \left(\frac{\bar{E}_f}{\bar{E}_s}\right)^{1/3} \quad (1)$$

where $\bar{E} = E/(1 - \nu^2)$ is the plane-strain modulus, E is the elastic moduli, ν is the Poisson's ratio (the subscripts f and s denote the PS film and PDMS substrate, respectively), and h_f is the film thickness. Using this relationship, we experimentally determined $\bar{E}_f$ for a flat PS film was 4.5 GPa, in agreement with previous studies.[19] To study the effect of the three geometric parameters described above, we systematically varied h_1, h_2, and d by employing different silicon molds and different solution concentrations. A summary of parameters used in this study as well as the resulting wrinkling wavelengths is listed in Table 1. There was no discernible dependence of λ on d within the range of pitch size examined in this study; however, if the pitch size was comparable to the wrinkling wavelength, then a dependency may be observed.[20] Thus, we concluded that h_1 and h_2 were the primary geometric parameters influencing the wrinkling wavelength in our system. As shown in Table 1, when the pattern height (h_2) is small compared to the residual film thickness (h_1), the difference between the wavelength of the perpendicularly oriented patterns and parallel oriented patterns is relatively small. However, this difference becomes more pronounced as the two layer thicknesses become comparable and is the largest when the pattern height is greater than the residual layer thickness.

The effect of geometric parameters h_1 and h_2 on the wrinkle wavelength can be better understood by a dimensional analysis. We first use eq 1 to calculate the wrinkling wavelength of a flat film of equivalent thickness (h_{eq}) that has the same volume as the nanopatterned film (see Figure S1, Supporting Information). We then define a dimensionless parameter λ/λ_{eq} and plot this parameter as a function of the ratio h_2/h_1, as shown in Figure 3a. The ratio h_2/h_1 can be thought of as a roughness ratio, as described previously.[21] This analysis demonstrates the inability of eq 1 to predict the wrinkling wavelength of a film with nanoscale roughness if one uses the "average" or equivalent thickness of the film as measured by, for example, ellipsometry or reflectometry. If the average thickness is used, eq 1 underestimates the wavelength if the pattern is aligned parallel to the compression direction and grossly overestimates the wavelength if the pattern is aligned perpendicularly, particularly at high ratios of h_2/h_1. Alternatively, we can define a different dimensionless parameter λ/λ_1, where λ_1 is the wavelength predicted by eq 1 if only the residual layer having thickness h_1 contributed to the wrinkling. We plot λ/λ_1 as a function on h_2/h_1 in Figure 3b. This analysis reveals the relative contribution of the pattern height (h_2) to the wrinkling wavelength. If the pattern height is small compared to the residual layer thickness (small h_2/h_1 ratio), the wrinkling wavelength is determined predominantly by the residual layer thickness and is relatively insensitive to the pattern orientation. When h_2/h_1 becomes large (tall patterns), we begin to observe a divergence between the parallel and perpendicularly oriented patterns. This divergence can be visualized by plotting the ratio $\lambda_\perp/\lambda_{//}$, a measure of anisotropy, as a function of h_2/h_1 as shown in Figure 3c.

To gain a quantitative understanding of the effect of geometry parameters and pattern orientation on the observed wrinkling wavelength, we propose a composite model that can approximate the effective properties of films with 1-D surface patterns. The equivalent thickness h_{eq} calculated earlier treated the film as isotropic and thus did not capture the orientational effects observed in the wrinkling wavelength. However, with unidirectional nanopatterns, the effective mechanical properties of the PS film are anisotropic. Similar to a fiber-reinforced composite lamina,[22] the effective mechanical properties of the patterned film can be obtained via a micromechanics approach, often known as rules of mixture. Considering that the feature size of the surface nanopattern is much smaller than the wrinkle wavelength, the patterned PS film may be treated as a continuous thin plate with effective in-plane and bending properties depending on the pattern geometry. Due to the thickness difference, the in-plane stiffness ($\sim Eh$) and the bending stiffness ($\sim Eh^3$) of the film are not uniform, and the effective properties can be obtained approximately by the rules of mixture with two phases corresponding to the two

dx.doi.org/10.1021/nl303512d | Nano Lett. 2012, 12, 5995−5999

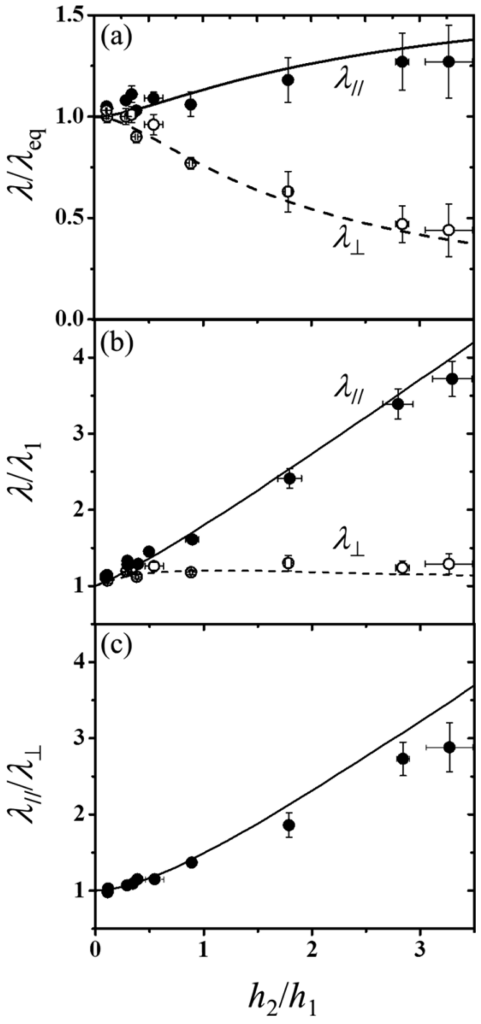

Figure 3. Effect of roughness ratio (h_2/h_1) on the wrinkling wavelength (λ) normalized either by (a) the wrinkling wavelength of a film with an equivalent thickness (h_{eq}) or (b) the wrinkling wavelength of a film comprised of only the residual layer (h_1). The two cases shown are when the pattern is either parallel ($\lambda_{//}$) or perpendicular ($\lambda_\perp$) to the compression direction. (c) Anisotropy in wrinkling depending on whether the pattern is parallel or perpendicular to the compression direction. The symbols in both graphs are experimental data, and the solid and dashed lines are the model prediction based on the effective thickness of the patterned film (h_{eff}).

thicknesses. The effective thickness of the patterned film is then obtained from the ratio of the effective bending stiffness to the effective in-plane stiffness. With the unidirectional line patterns, the effective mechanical properties depend on the compression angle. For perpendicular and parallel compression, the effective thicknesses are obtained as

$$h_\perp^{\text{eff}} = \sqrt{\frac{h_t^{-1}\phi + h_1^{-1}(1-\phi)}{h_t^{-3}\phi + h_1^{-3}(1-\phi)}} \quad (2)$$

$$h_{//}^{\text{eff}} = \sqrt{\frac{h_t^{3}\phi + h_1^{3}(1-\phi)}{h_t\phi + h_1(1-\phi)}} \quad (3)$$

where ϕ is the area fraction occupied by the line patterns ($\phi = 1/(1 + (L/S)^{-1})$ and h_t is the maximum total thickness of the film ($h_t = h_1 + h_2$). A more detailed formulation of eqs 2 and 3 can be found in the Supporting Information. For all experiments in the present study, L/S was kept constant at 1.4 and thus $\phi = 0.58$. These orientation-dependent effective thicknesses can then be used in conjunction with eq 1 to predict the wrinkling wavelengths of the nanopatterned films under perpendicular and parallel compression. As shown in Table 1, the wrinkle wavelengths calculated from the model were in good agreement with those measured experimentally within measurement error, validating the composite model. In particular, it is noted by eqs 2 and 3 that the observation of the wrinkle wavelength being independent of the pitch d is a direct result of the constant area fraction (ϕ) in all experiments. We overlaid the results of the composite model in Figure 3 (solid and dashed lines for parallel and perpendicular orientations, respectively), and the model accurately captured the effect of the pattern geometry and orientation on the wrinkle wavelength. Figure 3a shows that the two wrinkle wavelengths converge at small thickness ratios ($h_2/h_1 < 0.1$) to the wrinkle wavelength predicted by using the average thickness. This suggests that the use of average thickness is acceptable for predicting wrinkle wavelengths of thin films with relatively small surface roughness. However, when the roughness exceeds a critical value, the effect becomes significant and thus cannot be ignored. We further note that the composite model becomes less accurate for very high h_2/h_1 ratios, which is an intrinsic limitation of the model. Nevertheless, the composite model provides a valuable tool for understanding and predicting the anisotropic wrinkle wavelengths of the nanopatterned films. Future work will focus on a detailed angle dependence of wrinkling as well as the tunability of hierarchically wrinkled patterns with respect to the prepattern shape and wrinkling amplitude.

In summary, we demonstrated the wrinkling behavior of nanopatterned PS films, whose wrinkle wavelength and resultant morphology depend strongly on geometric parameters of surface patterns as well as the direction of the applied strain relative to the nanopattern orientation. The effect of the nanopattern on the wrinkle wavelength was more significant when the pattern was oriented parallel to the compression direction, resulting in an increase in the wavelength anisotropy for the higher h_2/h_1 ratios. The anisotropic wrinkling behavior of these nanopatterned films was interpreted quantitatively in terms of the effective thickness based on a composite model. We believe this study offers a simple route to design anisotropic hierarchical surface structures for potential applications including tunable wetting and adhesion, optics, and microfluidics. Our approach also provides insight into the effect of surface roughness on the wrinkle wavelength, which has direct implications in use of surface wrinkling to measure the mechanical properties of rough films.

■ ASSOCIATED CONTENT

Supporting Information

Experimental details; schematic illustrating the definition of equivalent thickness; detailed derivation of composite model. This material is available free of charge via the Internet at http://pubs.acs.org.

■ AUTHOR INFORMATION

Corresponding Author

*E-mail: chris.stafford@nist.gov; hyun.ro@nist.gov.

Present Address
[||]Center for Materials Architecturing, Korea Institute of Science and Technology, 39-1 Hawolgok-dong, Seongbuk-gu, Seoul 136-791, Republic of Korea.

Notes
The authors declare no competing financial interest.

■ ACKNOWLEDGMENTS

R.H. gratefully acknowledges financial support by the National Science Foundation (CMMI-1200161). P.L. gratefully acknowledges support under the NIST-ARRA Measurement Science and Engineering Fellowship Program (70NANB10H026). We thank Edwin P. Chan for his assistance with artwork. Equipment and instruments or materials are identified in the manuscript in order to adequately specify the experimental details. Such identification does not imply recommendation by the National Institute of Standards and Technology, nor does it imply the materials are necessarily the best available for the purpose. The error bars presented throughout this manuscript represent one standard deviation of the data, which is taken as the experimental uncertainty of the measurement.

■ REFERENCES

(1) Barthlott, W.; Neinhuis, C. *Planta* **1997**, *202*, 1.
(2) Lee, Y. W.; Park, S. H.; Kim, K. B.; Lee, J. K. *Adv. Mater.* **2007**, *19*, 2330.
(3) Liu, M. J.; Wang, S. T.; Wei, Z. X.; Song, Y. L.; Jiang, L. *Adv. Mater.* **2009**, *21*, 665.
(4) Zhang, F. X.; Low, H. Y. *Langmuir* **2007**, *23*, 7793.
(5) Koch, K.; Bhushan, B.; Jung, Y. C.; Barthlott, W. *Soft Matter* **2009**, *5*, 1386.
(6) Cortese, B.; D'Amone, S.; Manca, M.; Viola, I.; Cingolani, R.; Gigli, G. *Langmuir* **2008**, *24*, 2712.
(7) Ko, H.; Zhang, Z. X.; Takei, K.; Javey, A. *Nanotechnology* **2010**, *21*, 295305.
(8) Shirtcliffe, N. J.; McHale, G.; Newton, M. I.; Chabrol, G.; Perry, C. C. *Adv. Mater.* **2004**, *16*, 1929.
(9) Li, Y.; Huang, X. J.; Heo, S. H.; Li, C. C.; Choi, Y. K.; Cai, W. P.; Cho, S. O. *Langmuir* **2007**, *23*, 2169.
(10) Ming, W.; Wu, D.; van Benthem, R.; de With, G. *Nano Lett.* **2005**, *5*, 2298.
(11) Efimenko, K.; Rackaitis, M.; Manias, E.; Vaziri, A.; Mahadevan, L.; Genzer, J. *Nat. Mater.* **2005**, *4*, 293.
(12) Chiche, A.; Stafford, C. M.; Cabral, J. T. *Soft Matter* **2008**, *4*, 2285.
(13) Davis, C. S.; Crosby, A. J. *J. Polym. Sci. B: Polym. Phys.* **2012**, *50*, 1225.
(14) Wang, M.; Comrie, J. E.; Bai, Y. P.; He, X. M.; Guo, S. Y.; Huck, W. T. S. *Adv. Funct. Mater.* **2009**, *19*, 2236.
(15) Im, S. H.; Huang, R. *J. Mech. Phys. Solids* **2008**, *56*, 3315.
(16) Ohzono, T.; Shimomura, M. *Langmuir* **2005**, *21*, 7230−7237.
(17) Allen, H. G. *Analysis and Design of Structural Sandwich Panels*; Pergamon: New York, 1969.
(18) Groenewold, J. *Physica A* **2001**, *298*, 32.
(19) Stafford, C. M.; Harrison, C.; Beers, K. L.; Karim, A.; Amis, E. J.; VanLandingham, M. R.; Kim, H.-C.; Volksen, W.; Miller, R. D.; Simonyi, E. E. *Nat. Mater.* **2004**, *3*, 545.
(20) Ohzono, T.; Watanabe, H.; Vendamme, R.; Kamaga, C.; Kunitake, T.; Ishihara, T.; Shimomura, M. *Adv. Mater.* **2007**, *19*, 3229.
(21) Zheng, X. P.; Cao, Y. P.; Li, B.; Feng, X. Q.; Yu, S. W. *Comput. Mater. Sci.* **2010**, *49*, 767.
(22) Kaw, A. K. *Mechanics of Composite Materials*; Taylor & Francis: Boca Raton, FL, 2006.